Accepted Manuscript

Experimental investigation into the kinetics of Falcon UF concentration: Implications for fluid dynamic-based modelling

Q. Dehaine, Y. Foucaud, J-S. Kroll-Rabotin, L.O. Filippov

Please cite this article as: Q. Dehaine, Y. Foucaud, J-S. Kroll-Rabotin, L.O. Filippov, Experimental investigation into the kinetics of Falcon UF concentration: Implications for fluid dynamic-based modelling, *Separation and Purification Technology* (2019), doi: https://doi.org/10.1016/j.seppur.2019.01.048

Experimental investigation into the kinetics of Falcon UF concentration: Implications for fluid dynamic-based modelling

Q. Dehaine[1,2*], Y. Foucaud[1], J-S. Kroll-Rabotin[3], L.O. Filippov[1]

[1]Université de Lorraine, CNRS, GeoRessources laboratory, F54000, Nancy, France
[2]Camborne School of Mines, University of Exeter, TR10 9EF, Penryn, United Kingdom
[3]Université de Lorraine, CNRS, Institut Jean-Lamour, F54000, Nancy, France

[*] Corresponding authors: q.dehaine@exeter.ac.uk/quentin.dehaine@gmail.com
Phone: +44 (0) 1326 253602.

Abstract

Centrifugal gravity separators, such as the Falcon UltraFine (UF) concentrator, are the most common gravity concentration techniques used for fine particles processing. Hence, understanding the kinetics and separation mechanisms at play within these separators is of paramount interest. Recent research yielded a predictive physical model for the Falcon UF which however does not explain some results obtained with industrial ores. The Falcon UF kinetics have been investigated through the processing of fine-grained ores from the Altenberg tin deposit (Germany), the Tabuaço tungsten deposit (Portugal), a synthetic iron ore as well as results from previous studies on kaolin residues. Results have shown an evolution of Falcon UF performance with time/feed mass in contradiction with the stationary separation hypothesis on which the physical model was based. In terms of Falcon UF separation timing, four phases can be distinguished. First, upon initial feeding of the bowl, particles are trapped or rejected depending on their settling velocity. It yields a relatively ineffective selection according to density so that only ultrafine particles are ejected from the bowl, resulting in the quick growth of the concentrate bed. When the bed reaches a critical size, recovery and enrichment continue to increase through selective resuspension phenomenon that favours the concentration of dense particles and the ejection of larger particles. This way, the bed builds up while the content of concentrate bed surface evolves until resuspension balances the stream of dense material reaching the bed and recovery drops. The evolution of partition curves over time confirmed the low recovery of ultrafine particles during the whole operation but also showed a decrease of coarse particles recovery with time. It suggests that the second separation mechanism is less sensible to particle size compared to the first one and that size even has a negative impact on recovery. Furthermore, erosion figures in furrows are observed in the concentrate bed which may play locally an active role in the separation. These observations suggest that two separation mechanisms are at play. Firstly, differential particles settling within the flowing film which is already accounted for in the existing physical model. Secondly, resuspension of particles from the concentrate bed by the action of a lift force acting preferentially on coarse particles deposited at the surface of the bed and resulting in the rejection of coarser and lower-density particles. The addition of a lift force component to the existing model is discussed and a resuspension criterion is proposed as a guidance of the physics involved in this second separation mechanism. Future developments will require a dynamic model which would need to integrate the evolution of the concentrate bed content over time.

Key words: Gravity concentration, Centrifugal separation, Falcon concentrator, modelling, fine particle separation

1. INTRODUCTION

Enhanced gravity separators, which use additional centrifugal force to enhance the separation, are the most common gravity concentration techniques used for fine particles processing. Centrifugal separators can be seen as a ramification of the flowing film gravity concentrators category which employs centrifugal force to enhance the relative settling velocities of particles components [1]. These separators are mainly represented by the Knelson and Falcon concentrators as well as the Kelsey Jig and Multi Gravity Separator (MGS). The two latter devices actually use one additional separation mechanism, *i.e.* stratification for the Kelsey jig and shaking for the MGS. Falcon concentrators consist in a conical bowl capable of spinning at high rotation speed (up to 600 G), enabling the separation of fine particles based on their density [2]. The slurry is fed at the bottom-centre of the bowl and flows upwards along the bowl wall due to combined effect of bowl opening angle and centrifugal force. A retention zone delimited just before the bowl outlet retains the dense particles inside the bowl while the light particles are flushed over the top of the separator with the process water [3]. Three Falcon types are available industrially, namely, Falcon SB (Semi-Batch), Falcon C (Continuous), and Falcon UF (UltraFine), which differ by the way particles are trapped in the retention zone. Falcon SB series use fluidised annular grooves upstream of the bowl outlet to avoid compaction and adjust the retention capacity by injection of counter pressure water through the concentrate ridges. Falcon C series are operated on a continuous basis without any water addition due to subdivisions into hoppers with air operated valves to control the flow in the retention zone. Falcon UF concentrator series use a smooth bowl with a retention zone delimited by a slight reduction in diameter at the outlet, specifically designed to recover ultrafine particles (-5 µm). The bowl can be equipped with a variable lip in the retention zone to adjust its capacity [4]. No fluidisation counter-pressure is applied in these concentrators to prevent flushing out fine particles. Both Falcon SB and UF are operated in semi-batch mode and must be stopped before saturation of the bowl to avoid concentrate losses by erosion or by unselective separation [5,6]. Thanks to its design oriented towards ultrafine particles recovery, Falcon UF has been successfully employed to recover both metal-bearing heavy minerals (tin, tungsten, tantalum, chrome, and cobalt) and native metals (gold, silver) with particle sizes down to 3 µm [4]. Such performance however is material/ore-dependent and may vary from one mining operation to the

2

other. Hence, the development of a robust predictive model for Falcon UF separation performance considering both material properties and operating conditions would allow to optimise its overall performance, to control the quality of the concentration product or simply to assess the amenability of Falcon UF for a given application without the need for extensive trials.

Recently, fundamental modelling studies through numerical simulation methods such as Discrete Element Methods (DEM) or Computational Fluid Dynamics (CFD) have looked into the separation mechanisms as well as the influence of feed properties and operating parameters for Knelson contractors [7–10]. The separation process within Knelson and Falcon concentrators bowls relies on two main mechanisms, differential settling of particles in the flowing film along the inside wall of the bowl [5,11–14] and selective reorganisation of the particles in the retention zone through fluidisation [15,16], the latter being the predominant mechanism in Knelson concentrators [17]. However, since Falcon UF is not fluidised, this second separation mechanism is unlikely to occur in the smooth UF bowls as illustrated by the presence of a layer of denser material at the surface of the concentrate bed through the entire height of the bowl [18]. Hence, it is believed that there should be no reorganisation of particles in the concentrate bed, which leads to the model assumption that all the particles entrapped before saturation belong to the concentrate [19]. Based on a mechanistic understanding of the separation physics within those bowls, Kroll-Rabotin et al. [19–21] derived a physical model of the Falcon UF concentrator for diluted suspensions by solving a simplified particle transport equation analytically:

$$C_p = max\left(0,\ min\left(\frac{4\pi}{9}\lambda_0 Q^{-1}\omega^2\left(\rho_p\text{-}\rho_f\right)d_p^2\,\rho_f^{-1}\,\nu^{-1}R_{min}R_{max}H_{bowl},1\right)\right) \qquad (1)$$

in which C_p is the recovery to the concentrate, Q, and ω are the operating parameters (volume flow rate, and rotation rate), d_p and ρ_p are the particles properties (size and density), ρ_f and ν are the fluid density and kinematic viscosity, R_{min}, R_{max} and H_{bowl} are the dimensions of the bowl and λ_0 is a calibration constant. A full description of the forces acting on a particle within the Falcon UF bowl, as well as a detailed derivation of the model can be found in Refs. [19,20]. This model, which has been validated in laboratory conditions using pure-silica samples [22], relies on a number of assumptions, including the existence of a stationary separation stage before saturation and the no-resuspension of
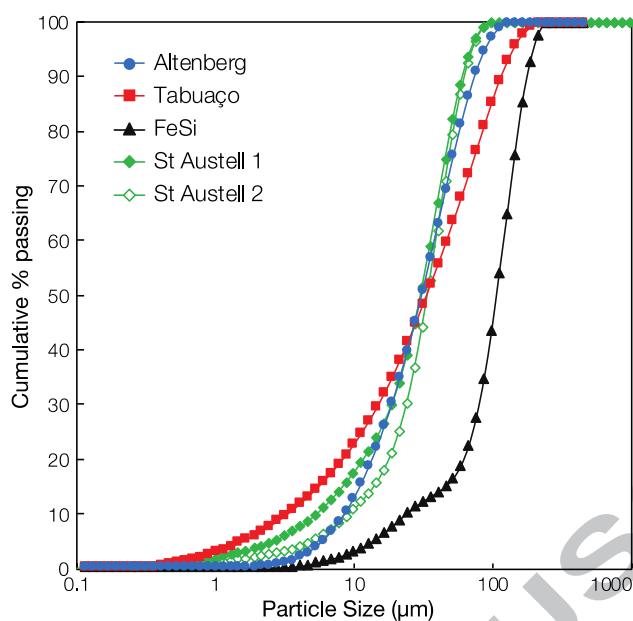
3

trapped particles in the bowl retention zone [19,20]. However, the model does not explain the increase in separation performance with time/feed mass before the bowl saturation as well as the potential evidences of resuspension as observed by some authors with industrial ores [6,11,12], who suggested that bed erosion phenomena may affect the efficiency of the separation over time.

This experimental study aims at identifying the mechanisms involved in Falcon UF centrifugal concentration with the objective of confirming or rejecting the hypotheses on which the current physical model is based, therefore defining its limitations and suggesting potential points of improvement. The third section presents experimental works used to question the stationarity of the separation and the no-resuspension hypothesis. Based on the conclusions drawn from these experiments, the fourth section presents a physical analysis of the separation under the new hypotheses, which leads to the integration of a resuspension component to the fluid dynamic-based model.
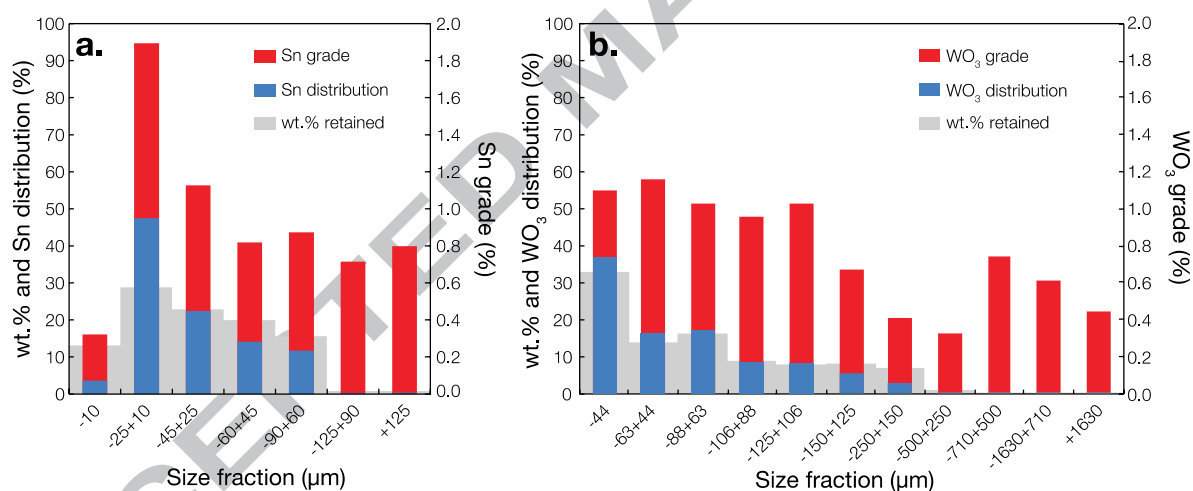
2. MATERIALS AND METHODS

2.1. Materials

The composite samples used in this study are considered to represent typical low-grade and fine-grained complex ores. They consist in a greisen-type tin (Sn) ore (Altenberg, Germany), a tungsten-bearing skarn ore (Tabuaço, Portugal) and a synthetic iron ore composed of a binary mixture of quartz and ferrosilicon (FeSi). All samples have been crushed using a laboratory jaw crusher and ground using a laboratory ball mill to reach suitable particle size for the tests (Figure 1). The Altenberg sample is a blend of 3 distinct facies with a mineralogy dominated by quartz, micas (zinnwaldite, biotite), feldspars and topaz with cassiterite (SnO_2) as the main Sn-bearing mineral, mostly distributed (47 wt.%) in the -25+10 µm fraction with a grade of 1.9% Sn (Figure 2a). The Tabuaço sample is mainly constituted of dense calcium-bearing silicates (vesuvianite, zoisite, grossular), fluorite, apatite and light silicates, mostly feldspars. Scheelite ($CaWO_4$) is the main host mineral, mostly distributed (50 wt.%) in the fine size fractions (-63 µm) with an average grade of 1.0% WO_3 (Figure 2b). The synthetic iron ore was obtained by mixing 50-200 µm pure quartz with -50 µm ferrosilicon (FeSi) with a 2:1 ratio.

4

Figure 1. Particle size distribution of the composite samples.

Figure 2. Grade and distribution by size-fraction in the Altenberg (a) and Tabuaço (b) composite samples.

2.2. Chemical analyses

Altenberg and Tabuaço samples were dried in an oven at 80°C, weighted and ground in a laboratory ring mill to obtain a -10 µm powder which was then riffled in representative aliquots. Chemical analyses were carried out by Energy Dispersive X-Ray Fluorescence spectroscopy (ED-XRF) using a Niton™ XL3t (Thermo Scientific) portable XRF analyser. External calibration of the XRF has been completed using duplicate analyses from Inductively Coupled Plasma Mass

Spectrometry (ICP-MS, Thermo Elemental X7) for the trace elements analyses performed at the *Service d'Analyses des Roches et des Minéraux* (SARM-CNRS, Nancy, France). Alternatively, the FeSi content of the iron synthetic ore was assessed by recovering the ferrosilicon particles from the test samples using magnetic separation and by weighting the magnetic and non-magnetic fractions with a precision scale.
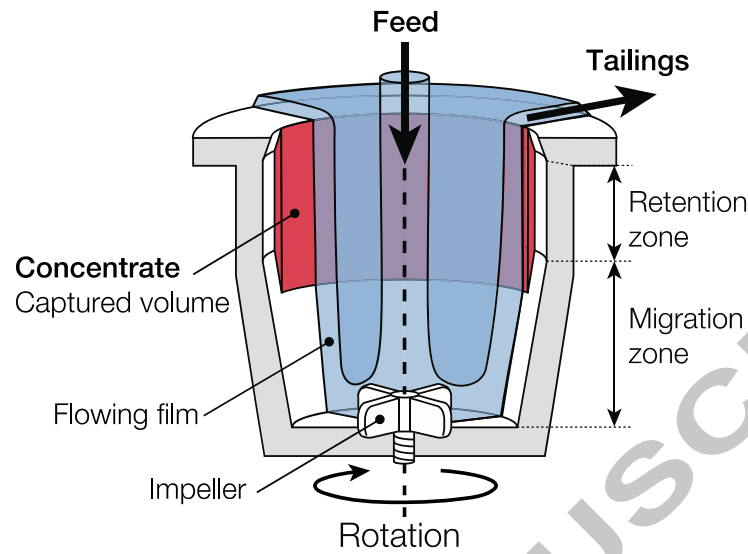
2.3. Particle size analysis

Particle size analyses were performed following two distinct techniques depending on the use of the size fraction. When the contents of each size fraction had to be separated for further analyses, particle size analysis was performed using a Rotap apparatus and a standard laboratory wet and dry sieving procedure (ISO 2591-1:1988). Alternatively, more detailed particle size analyses were obtained by laser light scattering using a Helium-Neon Laser Optical System Mastersizer 3000 (Malvern instruments Ltd.). The samples were introduced in a beaker coupled with a Hydro Extended Volume (EV), equipped with a dip-in centrifugal pump and a stirrer, until the desired obscuration level (up to 20%) was reached. The dispersed sample then passed through the measurement area of the optical bench, where a laser beam illuminated the particles. The obtained particle size distributions are the average of 5 duplicate measurements.

2.4. Falcon UF experiments

The Falcon concentrator used in this work is a Falcon L40 laboratory model (Sepro Mineral Systems, Canada). The device was operated in semi-batch and equipped with a 4" diameter ultrafine (UF) smooth-walled bowl (Figure 3). During the tests, the Falcon was run at 63.89 Hz (200 G's) and stopped at specific test durations, *i.e.* every 30 s for the first tests until 240 s and then at various durations depending on the material, to recover both concentrate and tailings. When the particle size distribution of the tailings was investigated, the Falcon was run continuously while tailings were recovered in different sample collectors during the experiment to account for the tailings produced at different duration of the experiment. Additional data from Filippov et al. [6], who investigated the recovery of Light Rare Earth Elements (LREE) from kaolin residues using the same apparatus, was used as a point of comparison. An overview of the materials and operating conditions for the

6

experiments can be found in Table 1.

Figure 3. Schematic cross-section of the Falcon L40 UF bowl modified after Refs. [6,22].

Table 1. Experimental design for the test series described in this study. For the St Austell tests, see Ref. [6].

Test series	Material					Operating conditions		
	Sample Type	D_{90} (µm)	Metal grade (%)	Host density (g.cm^{-3})	Gangue density (g.cm^{-3})	Rotary speed (G)	Pulp density (wt.%)	Flowrate (kg.min^{-1})
Altenberg	Greisen ore blend	78	~0.9	6.90	2.65	200	10	1.2
Tabuaço	Skarn ore	109	~0.5	6.00	3.4	200	11	1
FeSi	Synthetic ore	187	~24	6.53	2.7	200	2.5	3
St Austell 1	Kaolin residue	53	~0.04	5.15	2.6	200	10	1
St Austell 2	Kaolin residue (deslimed)	53	~0.04	5.15	2.6	200	10	1

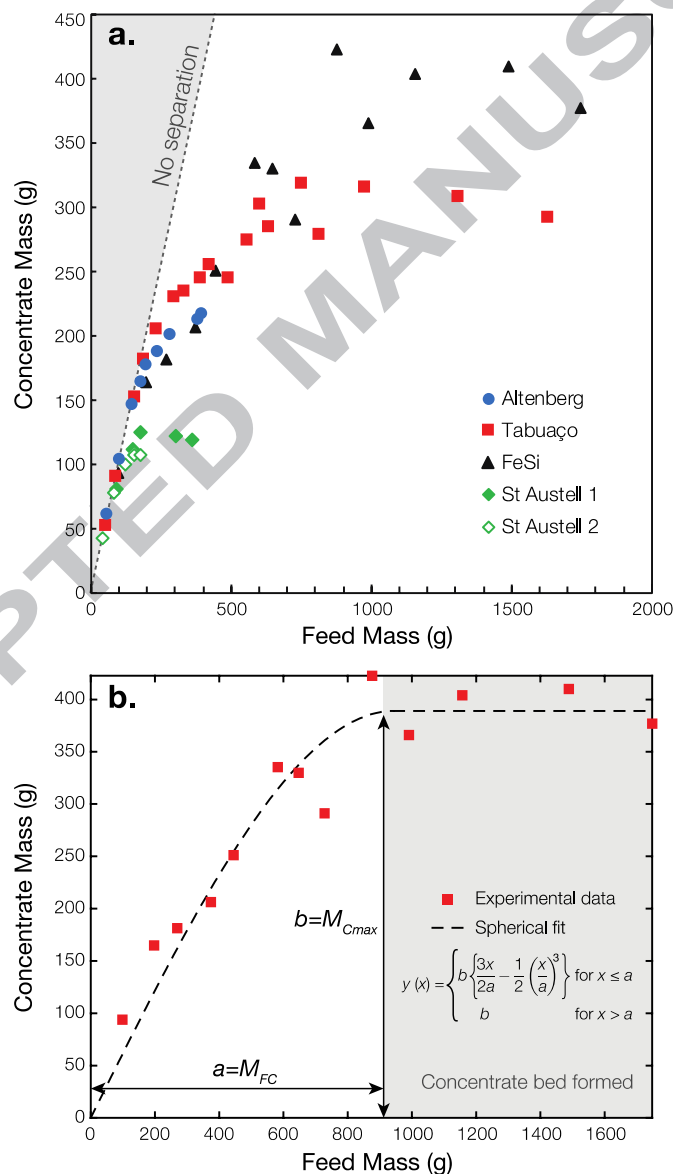## 3. EXPERIMENTAL RESULTS

3.1. Stationarity of separation performance with feed mass and time

Kinetic tests were conducted on all the samples with the Falcon UF by performing series of tests of various durations, each time recovering the concentrate and tailings for mass balancing and assaying. Figure 4a shows the evolution of the concentrate mass with the mass fed to the Falcon UF. All materials display a similar trend to the one observed in Ref. [6]. First, an initial phase occurs during which the concentrate mass is roughly equal to the feed mass, meaning that only desliming of the extremely fine fraction happens. This phase is followed by an increase of the concentrate mass at a

7

reduced rate until a plateau is reached, indicating that the concentrate bed attains its final profile. It should be noted that for the Altenberg sample however, no plateau is clearly reached, suggesting that additional experiments would be required to reach the maximum concentrate mass. Estimates of the critical feed mass (M_{FC}), *i.e.* feed mass after which the concentrate bed is maximum, as well as the corresponding maximum concentrate mass (M_{Cmax}), are obtained by fitting a spherical model to the saturation curve (Figure 4b). This fitting procedure is only used as a rigorous way to characterise the critical feed mass of each material and will not be used for any modelling purposes whatsoever.

Figure 4. Determination of the maximum concentrate mass and corresponding feed mass. (a) Falcon UF concentrate mass as a function of feed mass for all materials. (b) Illustration of the fitting procedure (here for the

FeSi sample) used to characterise the maximum concentrate mass and corresponding critical feed mass for each sample.

The critical feed mass obtained for each material and corresponding maximum concentrate mass are given in Table 2. It can be seen that these values depend on the characteristics of the materials and are also likely to be impacted by the operating conditions of each series of tests. These values vary drastically with an order of magnitude of up to 6 between the fine and low-grade St Austell 2 material, which displays the smallest maximum concentrate mass of 107.7 g at a critical feed mass of only 152.7 g, and the coarsest and highest-grade material, *i.e.* the synthetic iron ore (FeSi), which reached a maximum concentrate mass of 389.1 g at a feed mass of nearly a kilogram. The values given for the Altenberg sample are only indicative and may underestimate the maximum concentrate and corresponding critical feed mass as no clear plateau has been reached for this sample.

Table 2. Estimation of the maximum concentrate bed, corresponding critical feed mass and curves fitting summary.

Tests	Unit	Altenberg	Tabuaço	FeSi	St Austell 1	St Austell 2
Critical feed mass (M_{FC})	g	311.6	488.3	944.3	188.6	152.7
Max. concentrate bed mass (M_{Cmax})	g	210.2	286.8	389.1	121.9	107.0
Max. Yield (M_{Cmax}/M_{FC})	%	67.4	58.7	41.2	64.7	70.1
R^2	-	0.99	0.94	0.93	0.97	0.99

The critical feed mass obtained for each material can then be used to scale the results of each material by dividing the actual feed mass by the corresponding critical feed mass to reflect the bowl filling rate. A ratio of 100% corresponds to a feed mass equal to the critical feed mass, therefore suggesting that the concentrate bed reached its final profile and that the concentrate mass reached its maximum. It facilitates the comparison between the results from the different materials used in this study, regardless of their difference in terms of critical feed mass, and can be used as a reference to see the influence of the concentrate bed thickness on separation performance. The evolution of the Falcon UF separation performance in terms of enrichment ratio, yield and recovery with the % of critical mass (%M_{FC}) fed to the Falcon UF for all materials is shown in Figure 5a, 5b and 5c. Please note that enrichment ratio is used as a performance index instead of the concentrate grades as the latter vary drastically from one sample to the other (from hundreds of ppm for the St Austell sample to tens of
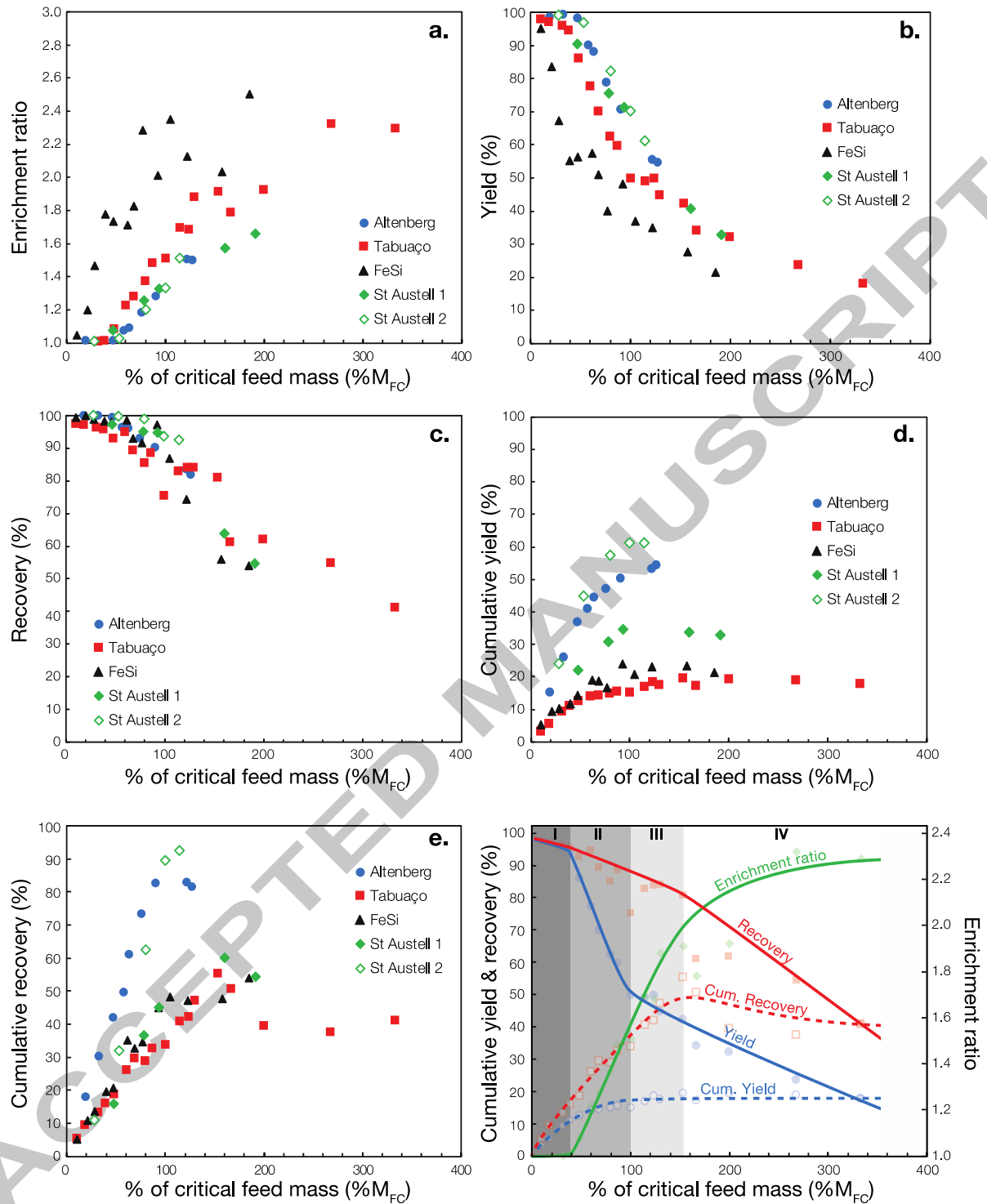
9

percent for the FeSi sample) making unpractical comparison between samples. For this reason, the variability of the enrichment ratio, in particular for FeSi, may be due to experimental error caused by slight variations in feed grade. For most materials, with the exception of the high-grade FeSi sample, the enrichment ratio stagnates around one (*i.e.* no concentration) for the very low feed masses (below 50 wt.% of critical mass) and then steadily increases with increasing feed mass up to a maximum at which it seems to reach a plateau (Figure 5a). On the contrary, the yield and recovery decrease with increasing feed mass, first at a very low rate for the very low feed masses and then at higher rate with an almost linear decrease (more important for the yield) until they suddenly break at distinct feed mass. The yield decreases almost linearly (much more quickly for FeSi) until the critical mass is reached and then decreases almost linearly again but at a lower rate than before the concentrate bed was formed (Figure 5b). This last linear decrease cannot be observed for the Altenberg and St Austell 2 samples due to lack of data after 100% critical feed mass. The recovery continues to decrease after the critical mass is reached until a certain feed mass depending on the characteristics of the material and then decreases almost linearly again but at a higher rate than before (Figure 5c). The rapid increase in enrichment ratio, as well as the rapid decrease in yield for the FeSi sample may be explained by its relatively higher grade and higher degree of liberation of the heavy fraction (theoretically 100%) compared to the other samples, as well as the high-density contrast between the heavy and the light fractions.

Cumulative recovery (or yield), at a given time *t* (or feed mass), are calculated by taking as a reference the last experiment (*i.e.* with the largest feed sample) of test duration *t*=T. Assuming that the weights and grades of the concentrate obtained for tests of lower duration (0<*t*<T) are representative of the variation of concentrate weight and grade with time/feed mass during the last experiment, cumulative recovery (or yield) would therefore reflects the kinetics of the separation. This is only an approximation which should be kept in mind when comparing these "cumulative" indexes, *i.e.* cumulative recovery/yield to the instantaneous ones, *i.e.* yield, recovery and enrichment ratios. The evolution of the cumulative yield and recovery with the % of critical mass fed to the Falcon UF is shown in Figure 5d and 5e. For all materials, cumulative yield increases with feed mass until it reaches a plateau at 100% critical feed while cumulative recovery continues to increase up to a maximum and

then it seems to slightly decrease and to reach a plateau too.

These observations contradict the stationary separation assumption upon which the current physical model is build. While previous works suggested the existence of three recovery phases [11,12], the results obtained in this study exhibit four separation phases during a batch Falcon UF operation as highlighted in Figure 5f using the results from the Tabuaço sample:

I. A first ineffective phase according to density for the first few tens of seconds of the operation during which almost no concentration occurs, the concentrate bed quickly grows and only differential settling impacts separation for the finest fractions which are ejected from the bowl (this corresponds to the steady regime modelled in Ref. [14]).

II. A second phase during which enrichment and cumulated recovery both increase while the cumulated yield quickly reaches a plateau, also highlighted by a break in the yield curve, indicating that the concentrate bed reached its final profile.

III. A third stage during which enrichment and cumulated recovery continue to steadily increase up to a point where cumulated recovery reaches a plateau, also indicated by a break in the recovery curve while enrichment ratio stabilises more gradually with increasing mass processed until it also reaches a plateau when the concentrate bed is saturated. This more gradual increase of the enrichment ratio compared to cumulative recovery is attributed to the aforementioned approximation used to calculate cumulative recovery as well as potential experimental errors associated with the enrichment ratio, as mentioned before.

IV. A fourth stage at which cumulative recovery, cumulative yield, and enrichment ratio stagnate, indicating that no more separation occurs and that the concentrate bed is saturated while yield and recovery continue to decrease, the latter at a more important rate than the yield, until ultimately reaching a near-zero value for very large feed masses, as observed by Ref. [12].
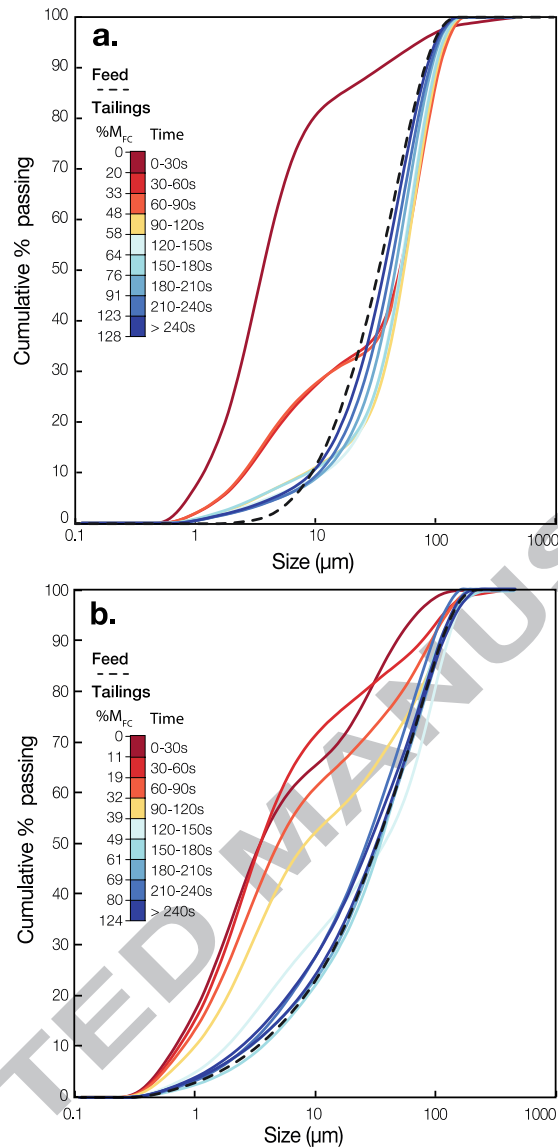
Figure 5. Effect of % of critical feed mass (%M_{FC}) on Falcon UF separation performance. (a) Enrichment ratio, (b) Yield, (c) Recovery, (d) Cumulative yield, (e) Cumulative recovery and (f) Overview for the Tabuaço sample with trend lines and identification of the distinct phases of the separation (see text for details).

3.2. Particle size effects

Additional tests were conducted, this time following the evolution of the particle size distribution (PSD) of the Falcon UF tailings with time for the Altenberg and Tabuaço samples (Figure 6). Results suggest that, during the first phase of the separation, mostly ultrafine (-10 μm) particles are rejected. After about 90-150s, depending on the material, corresponding to around 50% of critical feed mass *i.e*., during the second phase of the separation, the tailings display a much coarser PSD, which slightly translates towards the finer size ranges. It is clearly visible for the Altenberg sample, until its PSD becomes similar to the feed material PSD, when the concentrate bed reached its final profile at the beginning of the third phase of the separation.
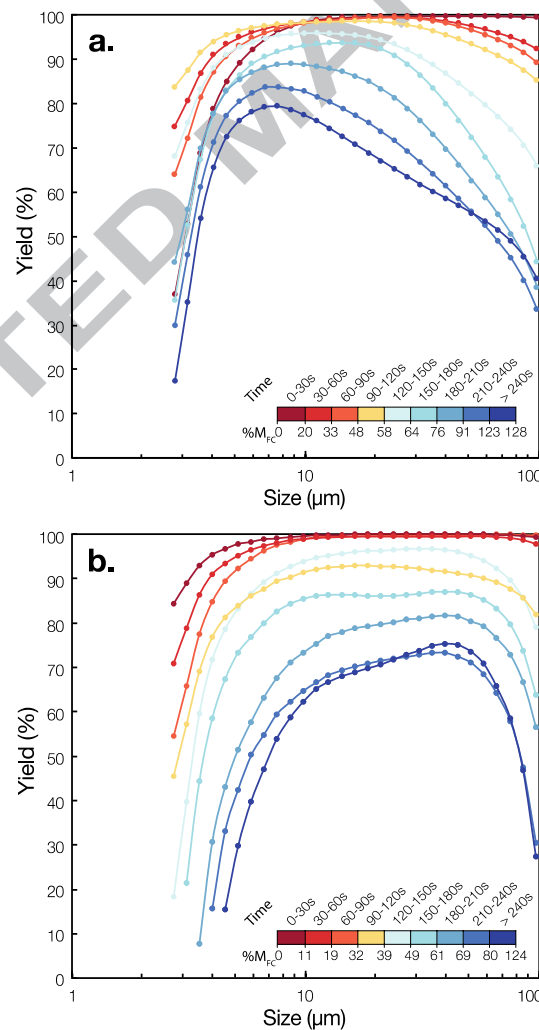
These results confirm those obtained by Kroll-Rabotin et al. (2012) with pure quartz, who showed that the tailings PSD remains unchanged for the first few minutes of the separation and then shifts towards the PSD of the feed [22]. This first phase of the separation during which ultrafine particles are rejected with a relatively constant PSD was taken to be a proof that the Falcon UF operates a steady state separation until the retention zone is full [22]. While it may be true for pure minerals, it seems that the opposite is observed here with more complex materials such as the industrial ores used in this study, exhibiting more heterogeneous compositions comprising high density metal-bearing minerals and gangue minerals displaying a range of low to medium specific gravities (Table 1). The first phase of the separation is actually non-selective from a metal-concentration point-of-view and only corresponds to a desliming phase during which the concentrate bed is still building up. The sudden increase in tailings PSD while cumulative recovery and enrichment ratio continue to increase could be evidence that actual gravity concentration still occurs after the bed is fully formed and that the effect of particle size becomes more limited.

Figure 6. Variation over time and % of critical feed mass (%M_{FC}) of the particle size distribution of the tailings of the Falcon UF concentrator for the Altenberg (a) and Tabuaço (b) samples.

Considering that the PSD of the feed remains constant during the experiment, the PSD of the tailings, along with the yields given in Figure 5, can be used to calculate the partition curve, *i.e.* the yield per size fraction, as a function of time for the Altenberg and Tabuaço samples (Figure 7). As expected, at the beginning of the operation, ultrafine particles (-5 µm) are ejected from the bowl. The concentrate bed is forming, the size recovery curves display a slightly decreased coarse particles recovery. These coarse particles losses drastically increase once the concentrate bed is formed, especially for the Altenberg sample. On the contrary, recovery at intermediate particle sizes, around 5-20 µm for Altenberg and 10-60 µm for Tabuaço, is higher during the whole operation. These features

14

are not without reminding those observed with spiral concentrators [23,24]. In such devices, the decrease in coarse particles recovery is attributed to the Bagnold force that preferentially flushes coarse particles towards the outer zone of the spirals through [25–27]. However, in the present study, the coarser size fractions are also depleted in dense particles as most of the tin and tungsten are distributed in the finer size fractions for the Altenberg and Tabuaço samples, respectively (Figure 2), which correspond to the size ranges of highest recovery when the concentrate bed is formed for both samples (Figure 7). Similar behaviour was observed by Laplante and collaborators processing gold ore flotation feed [12]. However, the same authors also reported the opposite behaviour using a Falcon B6 with synthetic magnetite-silica or gold-pyrite systems with a U-shaped partition curves for dense particles, *i.e.* lowest recovery at intermediate particle sizes [11,12].
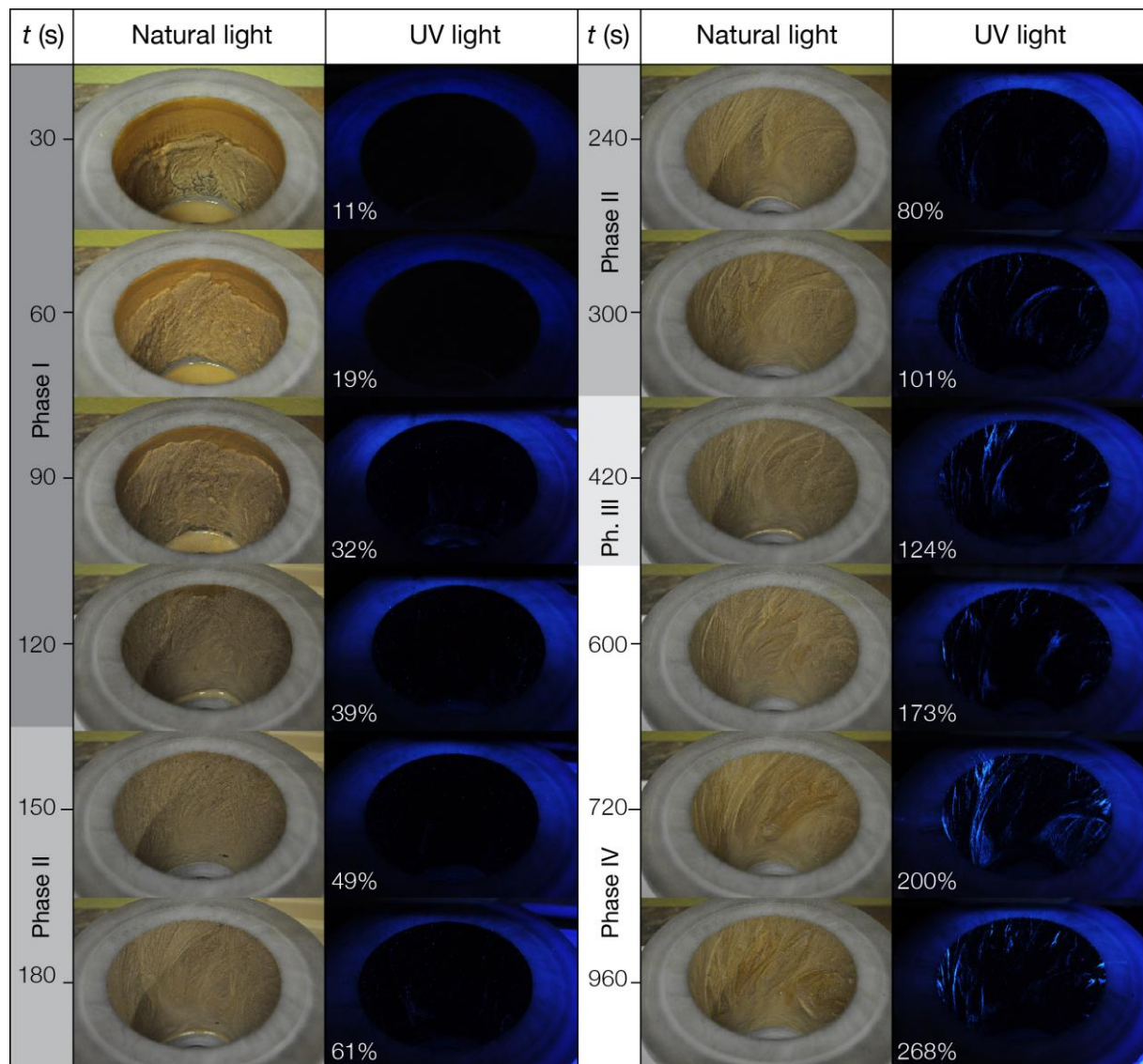

Figure 7. Variation over time and % of critical feed mass (%M_{FC}) of the partition curves of the Falcon UF concentrator for the Altenberg (a) and Tabuaço (b) samples.

3.3. Observations of the evolution of the concentrate bed during the operation

An examination of the Tabuaço concentrate bed within the Falcon UF bowl has been performed by marking the four cardinal points of the bowl and stopping the Falcon at different times. Figure 8 shows photographs of the concentrate bed at different times of the separation, *i.e.* at different % of critical feed mass, always pointing towards the same direction, with natural or ultraviolet (UV) light to reveal scheelite particles which fluoresce under short-wavelength UV light. It reflects the evolution of the concentrate bed during the four above-mentioned separation phases defined in Figure 5f. After 150 s, at 49% critical feed mass, phase II has just started, the concentrate bed is not yet completely formed and no clear concentration of scheelite is observed but rather some disseminated sparks, reflecting the composition of the feed. At 300 s, *i.e.* 101% critical feed mass, which corresponds to the transition between phase II and III, the concentrate bed has now reached its final profile and concentration of scheelite is clearly observed. Some erosion figures start to appear on the bed surface and observations under UV light suggest that scheelite is concentrated within these furrows. After 600 s, *i.e.* 173% critical feed mass, the furrows have changed positions indicating a local dynamic with erosion figures which are likely to evolve with time. From 720 s, *i.e.* 200% critical feed mass, some scheelite grains are observed on the edges of the bowl indicating scheelite losses to the tailings. The observed erosion figures correspond to the so-called furrows observed by Buonvino with a synthetic iron ore [11]. These furrows are created by the action of the slurry through the concentrate bed during its upward flow and, hence, may indicate preferential flow areas. This picture proves that the furrows actually play an active role in the separation as scheelite seems to be preferentially concentrated only within these furrows.
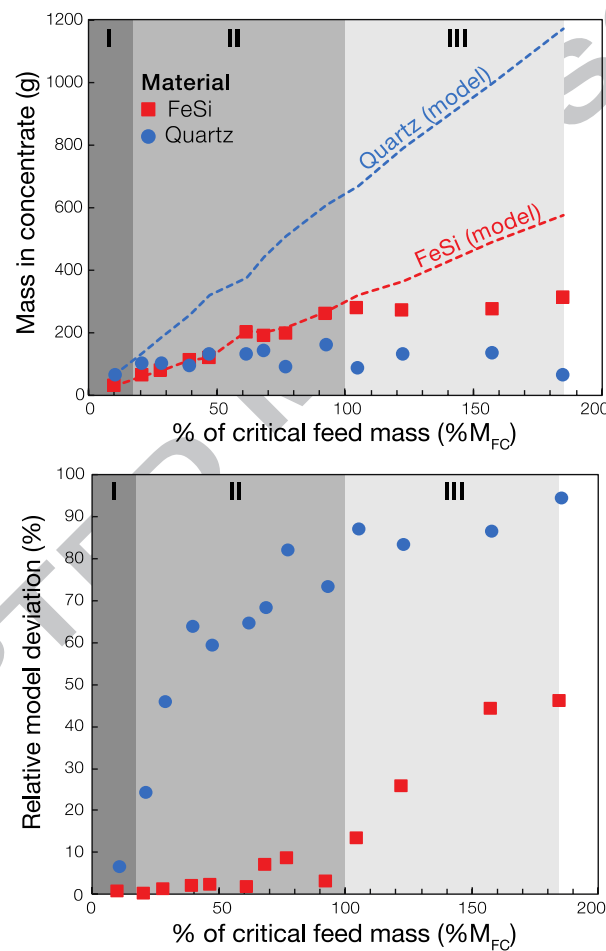
16

Figure 8. Photographs of the Tabuaço Falcon UF concentrate bed at different times of the separation or % of critical feed mass (non-linear scale) under natural or UV light with corresponding phases of separation as delimited in Figure 5f. All photographs are taken from the same angle, looking at the same direction.

4. IMPLICATIONS FOR THE FALCON UF PHYSICAL MODEL

The synthetic iron ore being constituted of set proportions of pure quartz and FeSi, the density and particle size distribution of which are known (see Table 1), the washability of this sample is thus fully characterised. Since the experimental conditions at which the Falcon UF tests were conducted are also known, it is possible to predict the recovery of both quartz and FeSi as well as their corresponding quantity in the concentrate using the current predictive model presented in Eq. (1). These values can then be compared with the mass of quartz and FeSi in the concentrate measured experimentally which

17

are easily obtained by recovering the FeSi particles with a magnet. Comparison of experimental and predicted quartz and FeSi masses in the concentrate shows that the predicted masses do not fit the experimental data for quartz and only partially until the last third of phase II for FeSi (Figure 9a). Indeed, from the first test, the relative model deviation for quartz sharply increases to reach up to 90% relative deviation while for FeSi, the relative model deviation stays below 10% for the first 7 tests (Figure 9b).

Figure 9. Comparison between experimental and predicted results for ferrosilicon (FeSi) and quartz using the Falcon UF physical model in Eq. (1) for the synthetic iron ore. (a) Predicted (dashed line) and observed (points/squares) concentrate mass as a function of %M_{FC}. (b) Relative model deviation compared to experimental results as a function of %M_{FC}.

From Figure 5 to 9, it can be inferred that two separation mechanisms are at play. The differential settling of particles within the flowing film is the one mechanism that has been accounted for in the

18

model developed by Kroll-Rabotin et al. [22], which is responsible for the ejection of fine particles during the whole separation cycle. However, the non-uniform decrease of the yield after the concentrate bed results from another mechanism. Hence the existing physical model should be valid for phase I and partially phase II as observed for FeSi in Figure 9. To fully account for phases II and III, another physical mechanism must be considered to explain how particles that have reached the bed (seen as trapped by the current model) may or may not be resuspended. Even, if the model seems to also apply to stage II for the FeSi, this is probably an artefact due to its very narrow size and density distributions.

Though the second mechanism does not achieve a steady state separation, it has been observed on Figure 9 that it is more sensitive to particle specific gravity and less to particle size compared to differential settling, and thus it improves the separation. This may be explained by the role of the lift force (F_L) that has been neglected in the physical model presented in Eq. (1). Indeed, when coarse particles reach the bed, the model assumes that they stay in it. Nevertheless, a fixed particle at the surface of the bed experiences a non-negligible slip velocity compared to the fluid, which, in combination with very high local shear rate, results in a potentially significant lift force when the flowing film is very thin, that is when the retention zone is filled. Lift force models for particles close to a wall are available in the literature, but with very large differences in terms of particle size contribution depending on the authors (exponents varying from 1.87 to 4 in the models listed in Ref. [28]), showing that the derivation of quantitative recovery models based on this force is still an issue. After listing many lift force models from the literature, Zeng et al. [28] provided their own, derived on numerical simulations of spherical particles close to a smooth wall. Although this situation is very idealistic compared to the mineral particles depositing in the retention zone of a Falcon concentrator, it gives a first approximation of the lift force undergone by the particles at the surface of the bed and how this force is impacted by the operating parameters. The lift force model by Zeng et al. [28] takes the following form:

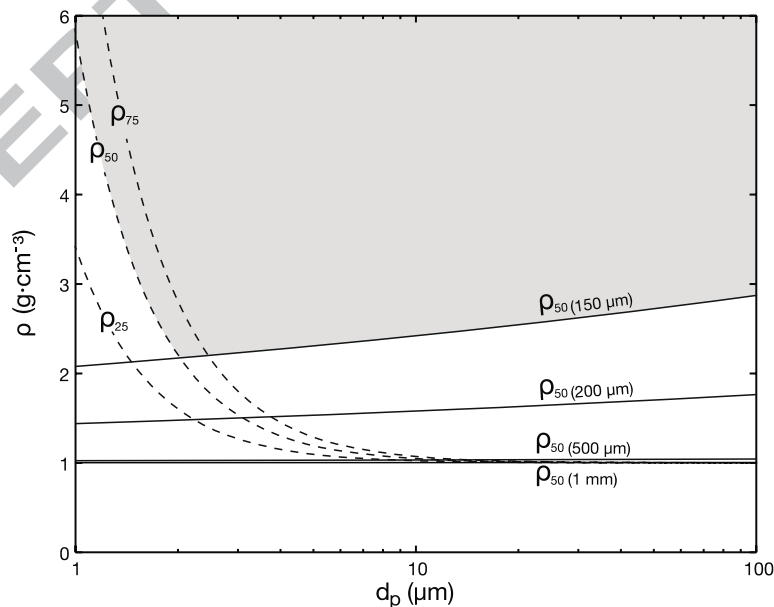$$F_L = 4.24\, \rho_f\, v^2 \left(\frac{1}{2} d_p \left(\frac{\gamma}{v} \right)^{1/2} \right)^{3.12} \tag{2}$$

where most parameters already appear in Eq. (1) and γ is the wall shear rate. Considering that this force mainly opposes particle apparent weight, and that the wall shear rate can be estimated from the analytically approximated velocity profile used in derivation of Eq. (1) [19], it yields a criterion to decide whether a given particle is able to stay immobile at the surface of the concentrate bed. A more detailed derivation of this criterion is provided in Appendix A. When lift force prevails over apparent weight, there is no equilibrium for such particles at the bed surface, which means that they either slide or roll on the bed surface or get transported by the flow and end-up being removed from the concentrate bed. This criterion can be turned into a very simplified separation curve, in the form of a cut surface, taking the value 1 when the particle stay at the surface of the concentrate bed and 0 when the particle is resuspended, the derivation of which can be found in appendix:

$$
C_p^L = \begin{cases} 1, & \rho_p > \rho_f \left(1 + 0.294\, \nu^{0.44} Q^{1.56} \omega^{-2} d_p^{0.12} R_{max}^{-2.56} h_{\text{film}}^{-3.12}\right) \\ 0, & otherwise \end{cases}
\tag{3}
$$

This separation curve has two noteworthy features. Firstly, the value of the cut density depends only very little on particle size (d_p has exponent 0.12), which means that the resuspension mechanism achieves a mostly density-based cut that is much less impacted by particle size than differential settling. Secondly, separation is strongly dependent on film thickness (h_{film}), which, in this part of the bowl, is directly related to the volume of concentrated material. As a consequence, separation according to this resuspension criterion varies during the operating cycle, as observed by Laplante et al. [12] and in section 3, unless the film thickness is controlled. This explains the observation and solution developed by Deveau [18] using an adaptive lip at the top of the bowl that grows during the separation cycle and maintains a more constant film thickness over time in the retention zone to control the separation while the bowl gets filled with concentrate.

Figure 10 shows the density cuts from the differential settling separation (C_p) defined in Eq. (1) and the lift induced separation (C_p^L) defined in Eq. (3) for various film thicknesses. The maximum realistic value for this thickness is a few millimetres, which is the depth of the retention zone when the bed is empty, at the beginning of an operating cycle. Its minimum value is the one of the flowing film flow induced by the fast rotation of the bow, which has been observed to go as low as 100 µm in the operating conditions of a laboratory scale Falcon UF [19]. The data in Figure 10 correspond to a

Falcon L40 unit that is not equipped with a varying lip retention zone. Figure 10 shows that the differential settling cut (in dashed line) is constant during a separation cycle but selective entrapment in the bed (continuous line) is not. As the retention zone gets filled with concentrate, the flowing film thickness decreases and the value of the cut density increases. The separation behaviour is thus transient and cannot be represented with a single cut surface. Future model developments will thus require a dynamic model. As a preliminary interpretation guide, Figure 10 shows a cut surface in grey colour that corresponds to the quasi static separation regime when the film is 150 µm thick. It means that when the bed is 150 µm thick, particles bigger than 10 µm with a density below approximately 2.5 g.cm^{-3} (below the grey area) will not be trapped, and that if such particles were trapped before and were close to the bed surface, they would be resuspended in the flow, which would in turn modify the height of the trapped bed and the film thickness. A very interesting result in regard to the performance of Falcon UF separation units is that the resuspension mechanism favours recovery of small particles with high density, as long as they are big enough not to be rejected due to the settling criterion. This is a strong asset to recover ultrafine particles compared to most other separation methods in which both density and size have a positive effect on recovery.

Figure 10. Cut functions corresponding to the differential settling mechanism (dashed line) and lift effect (solid line) for different flowing film thicknesses (in brackets). The two models are respectively defined in Eq. (1) and in Eq. (3), and are evaluated for a Falcon L40 with UF bowl operated at similar conditions to the FeSi

experiments, *i.e.* $Q = 3$ l/min and $\omega = 1863$ rpm (*i.e.,* 200 G).

The data presented in Figure 10 should not be read as quantitative, since the lift model by Zeng et al. [28] is only one among many and corresponds to an idealised case compared to the Falcon UF concentrate bed surface. For instance, the Bagnold effect is another way to explain the hydrodynamic lift experienced by particles under the influence of nearby boundary, fluid shear, and particle spin, which preferentially lifts particles into the higher velocity zones of the flowing film and that has more commonly been used to understand physical separation within gravity concentrators [26,29]. A discussion on the Bagnold force and how it compares to the lift force used here is provided in Appendix B. A quantitative model would need to integrate the evolution of the concentrate bed content over time and to be calibrated by experimental data. Moreover, when the flowing film becomes thin enough for resuspension to happen, its thickness gets close to the size of the resuspended particles, so a simple lift force model is not expected to capture the whole resuspension dynamics without corrective terms that will need to be calibrated from experiments. However, the simple resuspension criterion presented here gives a very interesting guide on what physics are at play and perform the separation in a Falcon UF bowl, for denser materials than the ones originally studied by Kroll-Rabotin et al. [19–22]. It provides a nice physical explanation to the experimentally observed improvement of the separation when the retention zone gets filled.

The four phases observed in section 3.1 can thus be interpreted as:

I. When the bed is not formed, the separation starts by a desliming-only phase that is controlled by differential settling in the flowing film;

II. As the concentrate bed grows, the flowing film gets thinner and shear increases in the flow, which makes particles at the surface layer of the bed undergo a lift force that is able to resuspend them into the tailings stream. The balance between this lift force and the enhanced gravity tends to suspend coarser and less dense particles first. During this phase, separation evolves from a differential settling driven selection to a resuspension driven selection;

III. When the bed is fully formed, the flowing film is very thin and highly sheared so that selective

22

erosion of the bed is strong and concentrate grade continues to increase although the mass of concentrate remains constant. During this stage, dense and fine particles enter the retention zone as coarser and less dense particles make room for them while being resuspended. This leads to the emergence of furrows of higher-grade material at the surface of the bed;

IV. As the surface layer of the bed contains higher-grade material and less gangue, the resuspension mechanism ejects more and more dense particles, until it balances the stream of particles settling at the bed surface and separation finally drops as the bed is saturated.

During all four stages, deposition of particles onto the bed is always governed by differential settling, which does not depend on the flowing film thickness [14], so that desliming of ultrafine particles stays the same.

5. CONCLUSIONS AND PERSPECTIVES

This experimental investigation into the kinetics of Falcon UF concentration contradicts the stationarity and the no-resuspension hypotheses on which the existing physical model is based. The evolution of Falcon UF performance indexes suggests a 4-phases separation. A first phase during which a bed quickly grows unselectively while ultrafine particles are ejected from the bowl. Then, a second phase where selective separation starts by differential settling while the concentrate bed quickly grows until it reaches its final profile. Next, a third phase starts, while the concentrate bed stabilizes, recovery and enrichment continue to increase through selective erosion phenomenon that seems to favour the concentration of dense particles. Finally, during the fourth stage, capture sites saturate and recovery drops. These results, combined with the evolution of partition curves over time, suggest the existence of two separation mechanisms: (i) differential particles settling within the flowing film responsible for the ejection of fine particles during the whole separation cycle which is already accounted for in the physical model, and (ii) resuspension of particles from the concentrate bed which may be explained by the action of lift force, neglected in the existing physical model. This force acts preferentially on coarse particles deposited at the surface of the bed, resulting in these particles being rejected in the tailings.

23

The addition of a lift force component to the existing model is discussed and a resuspension criterion is proposed as a guidance of the physics involved in this second separation mechanism. However, the future developments will require a dynamic model which would need to integrate the evolution of the concentrate bed content over time and to be calibrated on experimental data.

APPENDIX

Appendix A: Derivation of the resuspension criterion

Particle resuspension at the wall has been modelled (cf. Section 4) based on the expression of a lift force (F_L) from Ref. [28] and defined in Eq. (2), acting on a static particle deposited on a smooth wall. Such a lift force opposes the apparent weight of particles that results from the centrifugal force (F_C) and the buoyancy force (F_B) due to the density difference between the particles and the fluid (Figure A1):

$$F_c = \frac{\pi}{6} d_p^3 \omega^2 R_{max} \rho_p \qquad (4a)$$

$$F_B = \frac{\pi}{6} d_p^3 \omega^2 R_{max} \rho_f \qquad (4b)$$

A resuspension criterion for a given particle can then be written in the form of a cut surface, taking the value 1 when the particle stays at the surface of the concentrate bed and 0 when the force balance on the particle at the bed surface does not allow it to stay deposited. This can be summarised by the

24

following expression:

$$C_p^L = \begin{cases} 1, & F_L + F_B < F_C \\ 0, & otherwise \end{cases} \tag{5}$$

The cut surface for the resuspension criterion can then be expressed based on particles density:

$$F_L + F_B < F_C \Leftrightarrow F_L < \frac{\pi}{6} d_p^3 \omega^2 R_{max}(\rho_p - \rho_f) \tag{6}$$

$$\Leftrightarrow \rho_p > \rho_f \left(1 + 6\frac{4.24}{\pi}\frac{1}{2^{3.12}}\frac{v^2}{\omega^2 R_{max}} d_p^{0.12} \left(\frac{\gamma}{v}\right)^{1.56}\right) \tag{7}$$

Where the wall shear rate (γ) can be estimated from the analytical velocity profile used in derivation of

Eq. (1), using the approximation of a Poiseuille flow in the thin film flowing on the particle bed [19]:

$$\gamma = \frac{3}{2}\frac{Q}{2\pi R_{max} h_{film}}\frac{\partial}{\partial y}\left(1 - \left(\frac{y - h_{film}}{h_{film}}\right)^2\right)_{y=0} = \frac{3}{2}\frac{Q}{\pi R_{max} h_{film}^2} \tag{8}$$

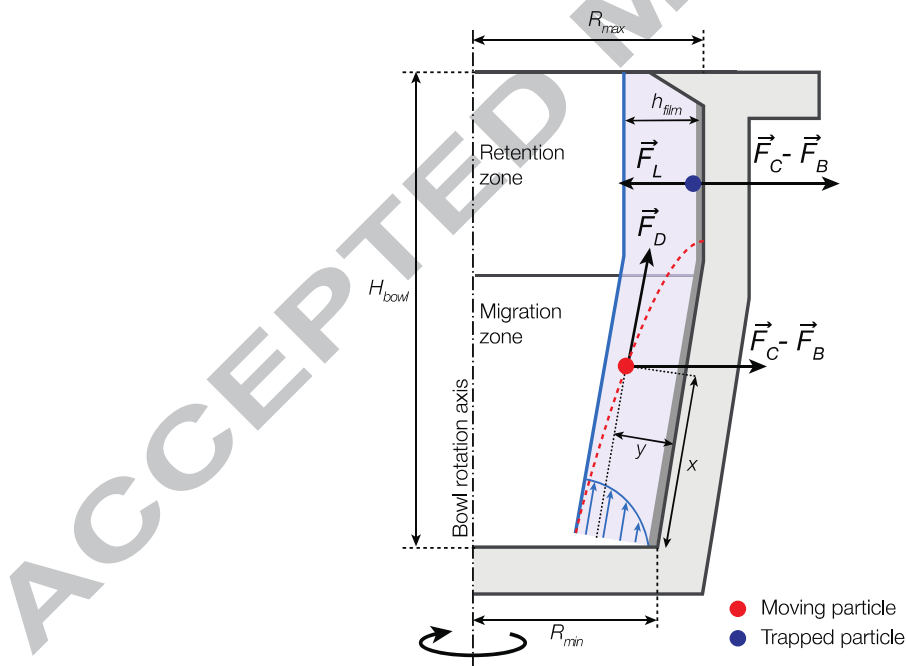where y is the normal distance of the particle from the wall (Figure A1).

Figure A1. Schematic cross section of the Falcon UF bowl showing the main forces controlling particles trajectory, *i.e.* the drag force (F_D), the centrifugal force (F_C), the buoyancy force (F_B) and the lift force (F_L), modified after Ref. [20].

Using the above definition for the wall shear rate, the cut density for the resuspension can then be

defined by the following expression:

$$\rho_p > \rho_f \left(1 + 6 \frac{4.24}{\pi^{2.56}} \left(\frac{3}{2}\right)^{1.56} \frac{1}{2^{3.12}} \nu^{0.44} Q^{1.56} \omega^{-2} d_p^{0.12} R_{max}^{-2.56} h_{\text{film}}^{-3.12} \right) \tag{9}$$

$$\Leftrightarrow \rho_p > \rho_f \left(1 + 0.294 \, \nu^{0.44} Q^{1.56} \omega^{-2} d_p^{0.12} R_{max}^{-2.56} h_{\text{film}}^{-3.12} \right) \tag{10}$$

It makes sense that the value of the density has a weak dependency on particle size, since the Falcon concentrator is a gravity-based separator and, as such, its separation principle is expected to be mostly sensitive to particles density rather than their size.

Appendix B: Discussion on the Bagnold force

The latter expression can be compared to Bagnold's formula for particle erosion due to saltation [30,31]. First, it is important to note that Bagnold's effect has been quantified from empirical results as a particle resuspension flux [26]. Defining such a flux would be useful to characterise the separation, but it does not fit well in the currently existing model that is expressed as a steady cut surface. A transient model will be necessary in the longer run since transient behaviour has been experimentally observed, but it will be a major evolution of the current model that will require its own set of experiments for calibration. Now, assuming that a direct relation exists between Bagnold's resuspension flux and the aforementioned resuspension criterion, the overall trends would be consistent: dependence on size has an exponent of 0.12 while Bagnold force expression would give a value between 0 "when the effects of fluid viscosity dominate" and 2 in turbulent transport [31,32] whereas the dependence on shear rate has an exponent of 1.56 while Bagnold's would be between 1 and 2 in the same respective flow conditions [31,32].

However, the resuspension criterion described in Eq. (3) is based on a static force balance on a deposited particle at the surface of the concentrate bed, while Bagnold's formula is empirical and accounts for erosion that is a combined effect from several mechanisms. Moreover, the Bagnold effect can vary significantly under different conditions and may not apply to particles deposited at the surface of the concentrate bed of a Falcon UF. Firstly, the apparent particle weight: in most Bagnold's derived erosion expression, particles are expected to be transported by the flow. In the situation of

26

very high gravity field, it is unlikely that so-called "resuspended" particles are actually transported in the film, they most probably slide or roll on the bed surface since the force balance does not allow them to stop at its surface. Secondly, the suspension rheology: Bagnold's effect assumes that there is a layer of solids flowing with the film in which collisions between the solids transfer stresses that are accounted for by an apparent rheology of the multiphase mixture. In a Falcon UF, if particles are not really resuspended but rather unable to remain at bed surface, there is no evidence that such a layer of solid-liquid mixture is flowing at the top of the bed. In addition, in the case of Falcon UF operation, the film Reynolds number is moderate, meaning that there is no turbulence to achieve dispersion of the solids in the film, and the gravity field is high, which means that settling prevails in the particle dynamics unless particles are stuck at the bed surface.

References

[1]   R.O. Burt, C. Mills, Gravity Concentration Technology, Elsevier Science Publishers, New York, NY, 1984.

[2]   A. Falconer, Gravity Separation: Old Technique/New Methods, Phys. Sep. Sci. Eng. 12 (2003) 31–48. doi:10.1080/1478647031000104293.

[3]   S. McAlister, K. Armstrong, Development of the Falcon concentrators, in: Soc. Mining, Metall. Explor. Annu. Meet., Orlando, Florida, 1998.

[4]   Sepro, Falcon UF Gravity Concentrators brochure, Sepro Miner. Syst. Website. (2015).

[5]   A.R. Laplante, N. Nickoletopoulos, Validation of a Falcon model with a synthetic ore, Can. Metall. Q. 36 (1997) 7–13.

[6]   L.O. Filippov, Q. Dehaine, I.V. Filippova, Rare earths (La, Ce, Nd) and rare metals (Sn, Nb, W) as by-products of kaolin production – Part 3: Processing of fines using gravity and flotation, Miner. Eng. 95 (2016) 96–106. doi:10.1016/j.mineng.2016.06.004.

[7]   L. Ma, L. Wei, X. Zhu, D. Xu, X. Pei, H. Xue, Numerical Studies of Separation Performance of Knelson Concentrator for Beneficiation of Fine Coal, Int. J. Coal Prep. Util. (2018) 1–11. doi:10.1080/19392699.2018.1434165.

[8]   M.R. Fatahi, A. Farzanegan, An analysis of multiphase flow and solids separation inside Knelson Concentrator based on four-way coupling of CFD and DEM simulation methods, Miner. Eng. 126

(2018) 130–144. doi:10.1016/j.mineng.2018.07.004.

[9]   M.R. Fatahi, A. Farzanegan, DEM simulation of laboratory Knelson concentrator to study the effects of feed properties and operating parameters, Adv. Powder Technol. 28 (2017) 1443–1458. doi:10.1016/j.apt.2017.03.011.

[10]   L. Ma, L. Wei, X. Pei, X. Zhu, D. Xu, CFD-DEM simulations of particle separation characteristic in centrifugal compounding force field, Powder Technol. 343 (2018) 11–18. doi:10.1016/j.powtec.2018.11.016.

[11]   M. Buonvino, A study of the Falcon concentrator, PhD Thesis, McGill University, 1993.

[12]   A.R. Laplante, M. Buonvino, A. Veltmeyer, J. Robitaille, G. Naud, A Study of the Falcon Concentrator, Can. Metall. Q. 33 (1994) 279–288. doi:10.1179/cmq.1994.33.4.279.

[13]   R.Q. Honaker, D. Wang, K. Ho, Application of the Falcon Concentrator for fine coal cleaning, Miner. Eng. 9 (1996) 1143–1156. doi:10.1016/0892-6875(96)00108-2.

[14]   R.L. Abela, Centrifugal concentrators in gold recovery and coal processing, in: Extr. Metall. Africa' 97, The South African Institute of Mining and Metallurgy, Randburg, South Africa, 1997.

[15]   A.K. Majumder, J.P. Barnwal, Modeling of enhanced gravity concentrators - Present status, Miner. Process. Extr. Metall. Rev. 27 (2006) 61–86. doi:10.1080/08827500500339307.

[16]   P. Ancia, J. Frenay, P. Dandois, Comparison of Knelson and Falcon centrifugal separators, in: R. Mozeley (Ed.), Innov. Phys. Sep. Technol. Richard Mozley Symp. Vol., IMM, Falmouth, United Kingdom, 1997: pp. 53 – 62.

[17]   A. Das, B. Sarkar, Advanced Gravity Concentration of Fine Particles : A Review, Miner. Process. Extr. Metall. Rev. 00 (2018) 1–36. doi:10.1080/08827508.2018.1433176.

[18]   C. Deveau, Improving fine particle gravity recovery through equipment behavior modification, in: 38th Annu. Meet. Can. Miner. Process., Ottawa, Canada, 2006: pp. 501–517.

[19]   J.-S. Kroll-Rabotin, F. Bourgeois, É. Climent, Fluid dynamics based modelling of the Falcon concentrator for ultrafine particle beneficiation, Miner. Eng. 23 (2010) 313–320. doi:10.1016/j.mineng.2009.10.001.

[20]   J.-S. Kroll-Rabotin, Analyse physique et modélisation de la séparation centrifuge de particules ultrafies en film fluant: application au séparateur industriel Falcon, PhD Thesis, Université de Toulouse, 2010. http://ethesis.inp-toulouse.fr/archive/00001549/01/kroll_rabotin.pdf.

[21]   J.-S. Kroll-Rabotin, F. Bourgeois, É. Climent, Physical analysis and modeling of the Falcon concentrator for beneficiation of ultrafine particles, Int. J. Miner. Process. 121 (2013) 39–50.

doi:10.1016/j.minpro.2013.02.009.

[22] J.-S. Kroll-Rabotin, F. Bourgeois, É. Climent, Experimental validation of a fluid dynamics based model of the UF Falcon concentrator in the ultrafine range, Sep. Purif. Technol. 92 (2012) 129–135. doi:10.1016/j.seppur.2011.10.029.

[23] Q. Dehaine, L.O. Filippov, Modelling heavy and gangue mineral size recovery curves using the spiral concentration of heavy minerals from kaolin residues, Powder Technol. 292 (2016) 331–341. doi:10.1016/j.powtec.2016.02.005.

[24] C. Bazin, M. Sadeghi, M. Bourassa, P. Roy, F. Lavoie, D. Cataford, C. Rochefort, C. Gosselin, Size recovery curves of minerals in industrial spirals for processing iron oxide ores, Miner. Eng. 65 (2014) 115–123. doi:10.1016/j.mineng.2014.05.012.

[25] Y. Atasoy, D.J. Spottiswood, A study of particle separation in a spiral concentrator, Miner. Eng. 8 (1995) 1197–1208. doi:10.1016/0892-6875(95)00084-4.

[26] P.N. Holtham, Particle transport in gravity concentrators and the Bagnold effect, Miner. Eng. 5 (1992) 205–221. doi:10.1016/0892-6875(92)90043-9.

[27] M. Sadeghi, C. Bazin, M. Renaud, Effect of wash water on the mineral size recovery curves in a spiral concentrator used for iron ore processing, Int. J. Miner. Process. 129 (2014) 22–26. doi:10.1016/j.minpro.2014.04.006.

[28] L. Zeng, F. Najjar, S. Balachandar, P. Fischer, Forces on a finite-sized particle located close to a wall in a linear shear flow, Phys. Fluids. 21 (2009) 033302. doi:10.1063/1.3082232.

[29] P.K. Jain, V. Rayasam, An analytical approach to explain the generation of secondary circulation in spiral concentrators, Powder Technol. 308 (2017) 165–177. doi:10.1016/j.powtec.2016.11.040.

[30] R.A. Bagnold, An Approach to the Sediment Transport Problem from General Physics, USGS Prof. Pap. (1966). doi:10.1017/S0016756800049074.

[31] R.A. Bagnold, Experiments on a Gravity-Free Dispersion of Large Solid Spheres in a Newtonian Fluid under Shear, Proc. R. Soc. A Math. Phys. Eng. Sci. 225 (1954) 49–63. doi:10.1098/rspa.1954.0186.

[32] T. Coulter, G.K.N. Subasinghe, A mechanistic approach to modelling Knelson concentrators, Miner. Eng. 18 (2005) 9–17. doi:10.1016/j.mineng.2004.06.035.
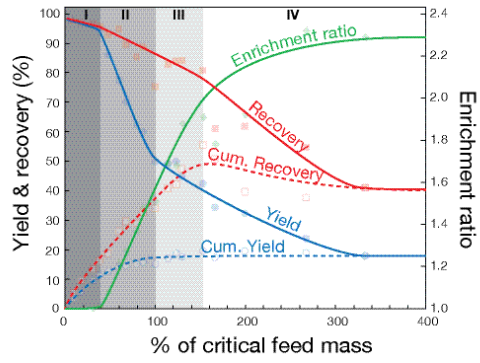
Highlights

- Falcon UF performance variation with time contradicts the stationarity hypothesis

- Four phases of separation have been distinguished

- Particle resuspension is observed contradicting the non-resuspension hypothesis

- A resuspension mechanism, more sensible to particle density, is proposed

- Addition of a lift force component to the existing model is suggested
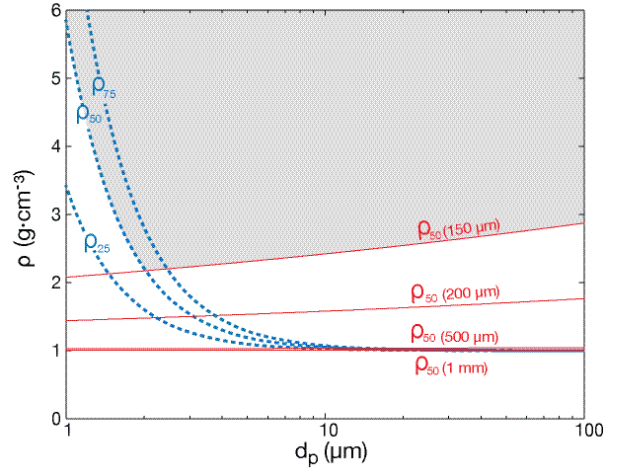
Phases of separation:
  I. Desliming: Differential settling only
  II. Differential settling > Resuspension
  III. Resuspension > Differential settling
IV. Saturation

Cut functions for the differential settling and resuspension models